A sensor for vector electric field measurements through a nonlinear anisotropic optical crystal

Luca Barbieri, Marco Gondola, Marco Potenza, Andrea Villa, and Roberto Malgesini

Citation: Review of Scientific Instruments **88**, 113114 (2017);
View online: https://doi.org/10.1063/1.4990861
View Table of Contents: http://aip.scitation.org/toc/rsi/88/11
Published by the American Institute of Physics

A sensor for vector electric field measurements through a nonlinear anisotropic optical crystal

Luca Barbieri,[1,a)] Marco Gondola,[1,a)] Marco Potenza,[2,a)] Andrea Villa,[1,a)] and Roberto Malgesini[1,a)]
[1]*RSE, Ricerca sul Sistema Energetico, Via Rubattino 54, 20134 Milano, Italy*
[2]*Dipartimento di Fisica, Università degli Studi di Milano, Via Celoria 16, 20133 Milano, Italy*

(Received 19 June 2017; accepted 30 October 2017; published online 29 November 2017)

Electrical applications require the development of electric field sensors that can reproduce vector electric field waveforms with a very large spectral width ranging from 50 Hz to at least 70 MHz. This makes it possible to measure both the normal operation modes of electrical components and abnormal behaviors such as the corona emission and partial discharges. In this work, we aim to develop a fully dielectric sensor capable of measuring two components of the electric field using a wide class of optical crystals including anisotropic ones, whereas most of the efforts in this field have been devoted to isotropic crystals. We report the results of the measurements performed at 50 Hz and with a lightning impulse, to validate the sensor. *Published by AIP Publishing.* https://doi.org/10.1063/1.4990861

I. INTRODUCTION

This work deals with the development of an optical, fully dielectric, electric field sensor capable of measuring two components of an impulsive electric field with a typical rise time of 1.2 μs and a fall time of 50 μs, i.e., the lightning waveform as specified in IEC 60060-1 international standards. We also aim to measure the electric field produced by alternated currents (ACs) at 50 Hz. These two requirements are mandatory to create a complete diagnostic instrument for high-power electric devices since the above cited bandwidth covers both normal operation modes and abnormal events such as partial discharges[1–3] and corona emission.[4–6] The main novelty of this work is the adoption of an anisotropic electro-optic crystal to fulfill the above-mentioned requests.

Similar measuring units have already been approached for technological applications in electrical power industry, for instance, in Refs. 7 and 8, the field close to a three bundle AC conductor has been measured, and in Refs. 9 and 10, some tests on electrical components are discussed. In Ref. 4, impulsive phenomena, such as the corona and partial discharges, have been considered, and in Ref. 11, the electro-optic technology has been applied to get a better understanding of the physics of lightning. Another very important application is the measurement of the field in electrical circuits as reported in Ref. 12.

In the literature, plenty of optical techniques for sensing electric fields are described (see Refs. 13–16 for a comprehensive review of this topic). Four technologies have mainly emerged: optical fibers impregnated with electro-optic crystals, interferometry, resonating cavities, and polarimetry measurements. The technology based on liquid crystals has been discussed, for instance, in Refs. 17 and 18. Unfortunately this method is quite ineffective at high frequencies and only provides the magnitude of the electric field.

On the contrary, the interferometric technology can be used to measure very high frequencies; in fact in some cases, it is used to substitute antennas. The transducing principle is based on the splitting of a laser beam into two beams, travelling different paths, and they are recombined downstream. One path is connected to an antenna, usually made up of metal. The properties of the light guides are properly chosen so that a distortion, proportional to the electric field, is impressed to the beam that passes through the shielded path. As the light is recombined, interference effects occur leading to the possibility of detecting the electric field. In Ref. 19, a tailored nanostructure is built on the transducer so that metallic parts are no longer needed. In spite of the impressive results obtained by this technique, detecting the direction of the electric field remains very difficult.

A similar technique, based on resonant cavities, aims at creating a proper interface between an optical fiber and an electro-optical crystal.[20,21] As the refractive index of the crystal changes accordingly to the electric field, the amount of light exchanged between the crystal and the fiber changes along with the total amount of light transmitted through the fiber. Except for a few cases,[22] this technique has not been actually exploited to measure the direction of the electric field.

The most adopted technology to match this requirement is polarimetry. As the light passes through an electro-optic crystal, its polarization state is changed, depending on the electric field. This technique makes it possible to measure the amplitude of the electric field along one direction with a relatively large rejection of the orthogonal components.[23] Temperature effects on the stability of the measurements have been analyzed in Ref. 24 where a proper automatic system is also studied to get rid of any problem resulting from large temperature variations. The optical scheme used in Ref. 23 has also been used in Refs. 25 and 26 to measure two components of the electric field using two separate sensing units placed side by side. Such a coupling may create undesired interference effects between the two transducers since a sensor may distort the electric field measured by the other one. A single unit capable of measuring

[a)]Authors to whom correspondence should be addressed: luca.barbieri@rse-web.it; marco.gondola@rse-web.it; andrea.villa@rse-web.it; roberto.malgesini@rse-web.it; and marco.potenza@unimi.it

two components at the same time has been developed in Refs. 27–30 where an isotropic crystal is used.

Very few applications of fully three-dimensional sensors exist. In Ref. 31, two technologies are combined for two dimensional and one dimensional measurements of the electric field (see Refs. 23 and 27–29). In this case, two sensors are placed side by side, and a detailed study of the interference effects is carried out using a finite element code. In Ref. 32, several laser beams are reflected through a proper crystal thus creating a three dimensional representation of the electric field. The crystal is placed in direct contact with an electric circuit to characterize its performances.

In this work, we study the measurement of two components of the electric field using a single crystal. This approach has many advantages over the use of two sensors sensitive only to a single component and potentially interfering. Moreover, as we are interested in signals that may have a large spectrum spanning from 50 Hz to tens of megahertz, it becomes mandatory to choose a crystal whose relative permittivity is as flat as possible depending on the frequency. Among the many crystals found in the literature (see, for instance, Refs. 33–38), we have chosen β-Barium-Borate (BBO) which provides one of the best frequency responses. BBO is anisotropic and has proper electro-optical coefficients. At the same time, it introduces additional challenges, as the single-shot measurement of two components with an anisotropic crystal is considered a difficult task (see, for example, Ref. 28). This work aims at overcoming these difficulties and developing a 2D vector sensor effectively, exploiting an anisotropic crystal. Moreover we have developed a proper sensing unit which contains almost all the optical units such as the electro-optic crystal and a couple of Wollaston prisms. As it will be detailed in the paper, this makes it possible to greatly simplify the overall sensor scheme as, with respect to Ref. 30, no real time closed-loop light frequency control is needed and only one polarization maintaining (PM) fiber is needed.

A general description of the optical scheme and the mathematical model of the sensor can be found in Secs. II A and II B. The sensor is made of a fully dielectric sensing unit connected through a bundle of optical fibers to an electronic signal treatment unit. The electronics have been developed *ad hoc* to maximize the performances of the device (Sec. II D). Laboratory tests have been carried out to validate the behavior of the complete unit as discussed in Sec. II E.

II. EXPERIMENTAL SECTION

A. Optical apparatus

The optical layout of the sensor is schematically represented in Fig. 1. Two different devices have been built:

1. a table-top mockup that has been used for the characterization of all the optical components and for the experimental evaluation of alignment requirements among the components. The full optical scheme has been tested on the optical bench;
2. a non-engineered assembled prototype, portable and stand-alone, to perform tests in relevant environments for the final application of the device.

The system is made of a linearly polarized, 10 mW He–Ne laser (wavelength $\lambda = 632.8$ nm, Thorlabs HNL050L-EC), delivering an almost Gaussian beam with a diameter of 0.65 mm. The beam is launched into a monomode, polarization maintaining (PM), optical fiber. The fiber has been coupled with a ferrule connector for physical contact (FC/PC) connector, on the laser side, and with a fully dielectric collimator on the other side. The latter has been engineered specifically by Thorlabs. The degree of polarization guaranteed by the fiber (99% approximately) is not enough for our aims; therefore, the light emerging from the collimator enters a Glan-Thompson (GT) polarizer that guarantees a high degree of rejection of the unwanted polarization components (10^{-5} rejection). A zero-order $\lambda/4$ plate ($\lambda/4$) provides circular polarization. It is useful to emphasize that, even if we introduce the GT polarizer, it is important to use a PM fiber to prevent the polarization changing due to stress induced birefringence into the fiber itself. In such a way, we guarantee the same polarization characteristics of the light entering the polarizer, and therefore, we maintain constant the intensity of light emerging from $\lambda/4$. The beam enters the nonlinear, Z-cut BBO crystal along the extraordinary axis. In the absence of an electric field applied, the beam emerges unchanged from the crystal. The beam is then split into two parts by the separation surface between two Wollaston prisms (W1, W2), as depicted in Fig. 1. The former is oriented in such a way to split horizontally the light polarized at 0° and 90°; the latter to split in the vertical direction the light polarized at 45° and 135°. The four emerging beams are collected by (purely dielectric) gradient index lenses (grin lens) and launched into four multimode fibers with a 100 μm diameter core. Each fiber delivers the light onto the sensible area of an avalanche photodiode connected to four electronic boards described in Sec. II D. The PM fiber connected to the laser and the four collection fibers is put into one bundle that, in turn, connects the measuring head to the control hardware unit. We have operated at a distance of up to 30 m from the head.

When the BBO crystal is placed in an electric field transverse to the optical axis, a birefringence arises proportionally to the field amplitude with a direction imposed by the field direction. The light emerging from the crystal and passing through the Wollaston prisms is therefore divided into four components

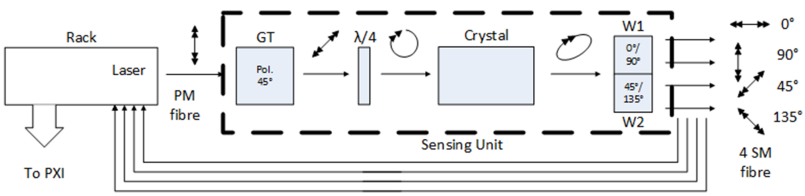

FIG. 1. Schematic representation of the optical configuration.

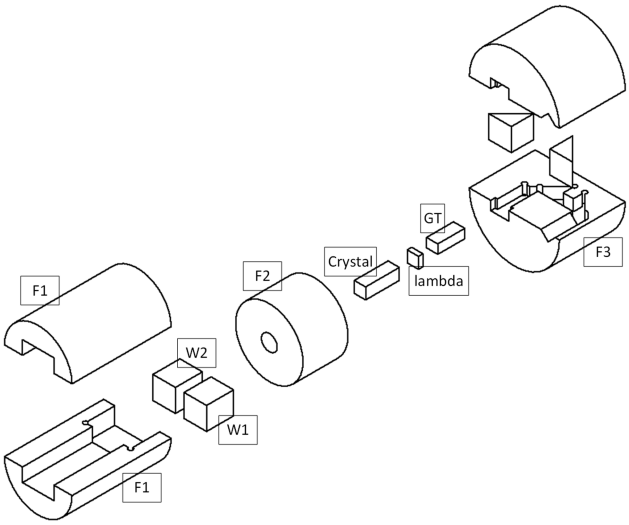

FIG. 2. The inner structure of the sensing unit.

with different intensities, delivering the information about the birefringence through the Stokes parameters measured by the four intensity values.

The BBO crystal has been selected due to its optical transparency, thermal stability, and stability of the dielectric permittivity at high frequencies. Refractive indices at the laser wavelength $\lambda = 632.8$ nm are $n_x = n_y = n_o = 1.6673$ for the two ordinary axes and $n_z = n_e = 1.5507$ for the extraordinary axis. BBO characteristics are described in Ref. 39. Here we consider a crystal cut in such a way that the light propagates along the extraordinary axis, and the crystal appears as a non-birefringent material in the absence of any applied field.

The holder of the sensing unit consists of three parts as depicted in Fig. 2. The two external parts (F1, F3) have been built using polylactic acid (PLA) for 3D printing two halves of the cylindrical structures. The holder of the BBO crystal (F2) has been turned on a lathe using polyethylene plastic. It is a cylinder concentric to the optical axis with a cylindrical hole specifically designed to hold the BBO crystal. This reduces the interface gap in the dielectric constant (see below). The crystal is a square-based prism that is held on the sides. This creates an air gap between the holder F2 and the crystal that has some critical effects on the measurements. We have specifically studied how this affects the measure of the external field by means of finite element (FE) modeling. In particular, we aim to

1. design the holder to minimize spurious information from polarimetry measurements;
2. obtain a detailed knowledge of the measured birefringence in the presence of the holder, in order to be able to invert the problem and determine the external, undisturbed field;
3. guarantee a very tight alignment between the two Wollaston prisms and the BBO crystal. In fact, the laser beam is collimated so as to be exactly split into two parts by the interface between the two prisms, thus preventing the use of any beam splitter that has, in general, negative effects on the polarization.

The geometry of the sensor has been optimized to minimize the spurious effects on the electric field. In particular, it is important that the electric field in the central part of the crystal, i.e., the region passed by the laser beam, is aligned with the imposed electric field. In Fig. 3, we have depicted the electric field directions considering different relative orientations of the crystal axes with the imposed, external electric field. Results show that the electric field is just slightly distorted in the interface regions between the crystal and the surrounding air gap, while in the central part of the crystal the field is well aligned with the external one. Moreover the particular mechanical coupling between the crystal and the holder makes it possible to obtain a relatively high electric field amplitude in the crystal. This is a critical issue since most of the electro-optic crystals have a very large relative permittivity which implies a large abatement of the field strength inside the crystal.

The particular configuration employed guarantees that the electric field in the gap between the crystal and the holder is higher than the external applied field. On average, it is 1.34 times the external field, and the field in the core of the crystal is about 0.299 times the external electric field. This ratio is much larger than the ratio between the air permittivity and the permittivity of the BBO, which is close to 1/6. Also the modulus of the electric field is very stable for different orientations of the crystal with respect to the applied electric field. We have considered the configurations depicted in Fig. 3, and we have computed the relative changes of the electric field in the centre of the BBO with respect to the external applied electric field. As we can see in Table I, the difference is below 1%.

Moreover the particular choice of aligning the laser beam with the extraordinary axis gives an intrinsic stability with respect to temperature. The two refraction indexes perpendicular to the laser beam are equal and change in the same manner with temperature. Furthermore the stability of the indexes of BBO is very high and does not change substantially in the

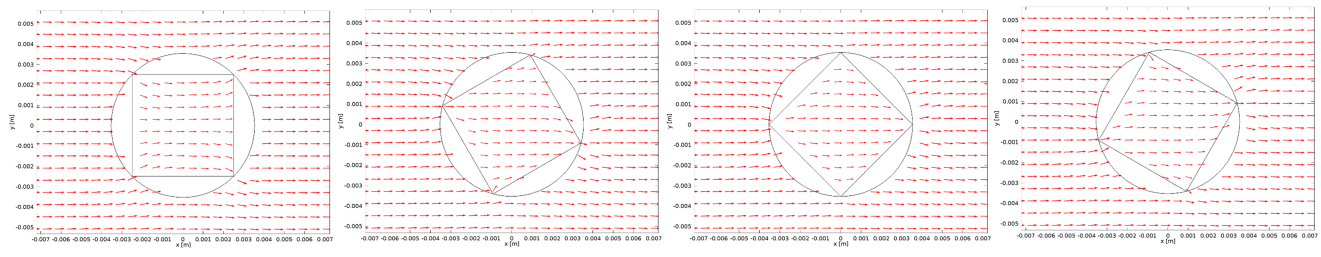

FIG. 3. The directions of the electric field in the crystal considering different angles.

TABLE I. Deviation of the modulus of the electric field in the center of the crystal due to the relative rotation of the crystal with respect to the external applied electric field.

Variation	Rotation (deg)
0	0
5.26×10^{-4}	30
3.68×10^{-3}	45
6.32×10^{-3}	60
7.89×10^{-3}	75
1.06×10^{-2}	90
5.26×10^{-3}	135
0	180

range 0–60 °C which is the temperature range envisaged for the sensor (see Ref. 39).

With respect to similar configurations, such as the one described in Ref. 30, we have embedded almost all the optical components in the measuring head. This requires the use of five fibers instead of the two fibers used in Ref. 30; however, we require only one polarization maintaining fiber, while the other four are multi-mode fibers which are very common and cheap. Our particular configuration does not require any closed-loop control, which, on the contrary, was used in Ref. 30 along with a laser with a tuneable frequency. In our case, a less-complex, fixed frequency laser can be used.

B. Crystal model

As we have already pointed out, we use a BBO crystal Z-cut with the extraordinary axis aligned with the laser beam. The electro-optical tensor is described by the following matrix:

$$\begin{bmatrix} 0 & -r_{22} & r_{13} \\ 0 & r_{22} & r_{13} \\ 0 & 0 & r_{33} \\ 0 & r_{51} & 0 \\ r_{51} & 0 & 0 \\ -r_{22} & 0 & 0 \end{bmatrix}, \tag{2.1}$$

where $r_{13}, r_{22}, r_{33}, r_{51}$ are its components. As a consequence, the permittivity tensor on the plane x–y, which is perpendicular to the axis of propagation of the laser beam, can be expressed by

$$\begin{bmatrix} \alpha & \phi \\ \phi & \beta \end{bmatrix}, \tag{2.2}$$

where

$$\alpha = \frac{1}{n_o^2} - r_{22}E_y + r_{13}E_z, \quad \beta = \frac{1}{n_o^2} + r_{22}E_y + r_{13}E_z, \quad \phi = -r_{22}E_x, \tag{2.3}$$

where E_x, E_y, E_z are the components of the external applied electric field. The eigenvalues of matrix (2.2) define the actual refractive indices $n_\pm$ of the crystal, see Refs. 15, 16, and 40, and the matrix of eigenvectors implicitly defines the rotation angle ψ, see Fig. 4.

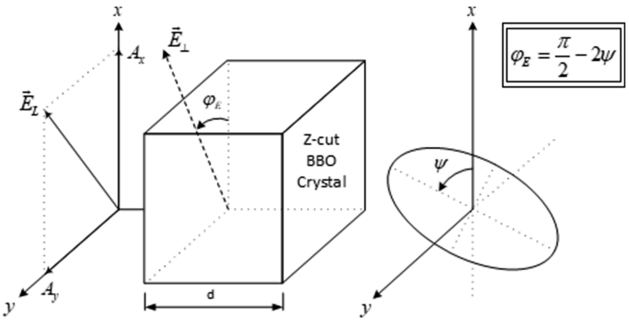

FIG. 4. Representation of the characteristics of the electric field associated with the light propagation and the external electric field.

With a few algebraic manipulations, we get

$$n_\pm = n_o\left(1 + n_o^2 r_{13}E_z \pm n_o^2 r_{22}\left|E_\perp\right|\right)^{-\frac{1}{2}}, \quad \tan(2\psi) = \frac{2\phi}{\alpha - \beta}, \tag{2.4}$$

where $E_\perp$ is the projection of the electric field vector $\vec{E}$ on the plane x–y which is perpendicular to the laser beam. Since, even at high electric fields, $n_o^2 r_{13}E_z \ll 1$ and $n_o^2 r_{22}\,|E_\perp| \ll 1$, the first equation of (2.4) can be simplified obtaining

$$n_+ = n_o + \delta n_+, \quad n_- = n_o + \delta n_-, \tag{2.5}$$

where

$$\delta n_+ = -\frac{1}{2}n_o^3 r_{13}E_z - \frac{1}{2}n_o^3 r_{22}\left|E_\perp\right|,$$
$$\delta n_- = -\frac{1}{2}n_o^3 r_{13}E_z + \frac{1}{2}n_o^3 r_{22}\left|E_\perp\right|. \tag{2.6}$$

Now, substituting definitions (2.3) into the second equation of (2.4), we have

$$\tan(2\psi) = \frac{-2r_{22}E_x}{\frac{1}{n_o^2} - r_{22}E_y + r_{13}E_z - \frac{1}{n_o^2} - r_{22}E_y - r_{13}E_z} = \frac{E_x}{E_y}. \tag{2.7}$$

Thus defining $\tan(\varphi_E) = \frac{E_y}{E_x}$, we get

$$\tan(2\psi) = \frac{1}{\tan(\varphi_E)}. \tag{2.8}$$

This correlates the directions of the electric field to the rotation of the reference system in which the permittivity matrix is diagonal. We also point out that the birefringent effect is given by

$$\delta n_- - \delta n_+ = n_o^3 r_{22}\,|E_\perp|, \tag{2.9}$$

and thus it depends only on the modulus of the projection of the electric field on the x–y plane, while it does not depend on the electric field direction.

C. Polarimetry

We now describe the variation of the light polarization due to the electric field. We consider the crystal and the Wollaston prisms depicted in Fig. 2. They act as an ideal polarizer so that in Fig. 5 we have considered the ensemble of these two elements as a representative of one of the four measured channels.

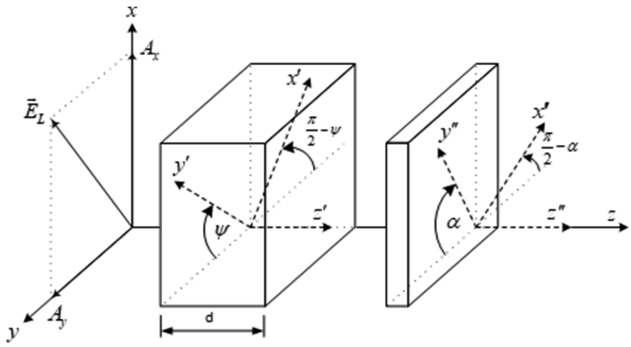

FIG. 5. The crystal and a linear polarizer.

The laser beam enters the crystal with a circular polarization; therefore, the electric field associated with the propagation of the light is described, using the Jones formalization,[40,41] by the vector $\vec{E}_L = [A_x e^{i\delta_x}, A_y e^{i\delta_y}]$, where A_x, A_y are the intensities of the x and y components of the electric field associated with the light and δ_x, δ_y are the phases such that $\delta_x - \delta_y = \pi/2$. The light exiting the optical assembly is described by

$$\begin{bmatrix} E^{out}_{L,x} \\ E^{out}_{L,y} \end{bmatrix} = R(\alpha) \mathrm{M}_p R(-\alpha) \mathrm{R}(\psi) \mathrm{M}_c R(-\psi) \begin{bmatrix} A_x e^{i\delta_x} \\ A_y e^{i\delta_y} \end{bmatrix}, \quad (2.10)$$

where $E^{out}_{L,x}$, $E^{out}_{L,y}$ are the two components of the electric field associated with the light just after the linear polarizer, α is the angle of the polarizer, and

$$R(\alpha) = \begin{bmatrix} \cos(\alpha) & -\sin(\alpha) \\ \sin(\alpha) & \cos(\alpha) \end{bmatrix}, \; M_p = \begin{bmatrix} 1 & 0 \\ 0 & 0 \end{bmatrix}, \; M_c = \begin{bmatrix} e^{ik_x d} & 0 \\ 0 & e^{ik_y d} \end{bmatrix}, \quad (2.11)$$

where d is the length of the crystal, $k_x = \frac{2\pi}{\lambda} n_x$, $k_y = \frac{2\pi}{\lambda} n_y$, λ is the laser wavelength in vacuum, and n_x, n_y are the two refractive indices of the crystal defined as $n_\pm$ in Sec. II B. The intensity of light can be computed as

$$I = \begin{bmatrix} E^{out}_{L,x} \\ E^{out}_{L,y} \end{bmatrix}^* \begin{bmatrix} E^{out}_{L,x} \\ E^{out}_{L,y} \end{bmatrix}, \quad (2.12)$$

where * indicates the adjoint operator. In our case, we perform four measures: $I_0, I_{90}, I_{45}, I_{135}$ corresponding to four different angles, i.e., $\alpha = 0°, 90°, 45°, 135°$. From these, we can compute the following Stokes parameters, see Ref. 40:

$$S_1 = I_0 - I_{90}, \quad S_2 = I_{45} - I_{135}. \quad (2.13)$$

Substituting (2.10) into (2.12) and performing some algebraic manipulations, we obtain

$$\begin{aligned} S_1 &= -S_0 \sin(2\psi) \sin\left[\left(k_y - k_x\right) d\right], \\ S_2 &= S_0 \cos(2\psi) \sin\left[\left(k_y - k_x\right) d\right], \end{aligned} \quad (2.14)$$

where $S_0 = 2A^2 = 2\left(A_x^2 + A_y^2\right)$. Dividing the two equations of (2.14), we get

$$\psi = -\frac{1}{2} \arctan\left(\frac{S_1}{S_2}\right). \quad (2.15)$$

Once we have determined the angle ψ and substituting back in one of the equations (2.14), the birefringence turns out to be

$$d\left(k_y - k_x\right) = 2\pi \frac{d}{\lambda}\left(n_y - n_x\right) = 2\pi \frac{d}{\lambda}\left(\delta n_y - \delta n_x\right). \quad (2.16)$$

Using Eqs. (2.15) and (2.8), the direction of the electric field can be computed. Moreover using Eqs. (2.16) and (2.9), the modulus of the electric field in the x–y plane can be deduced. We point out that, from an experimental point of view, the birefringence in Eq. (2.16) can be deduced either by S_1 or S_2. If both signals have a good signal to noise ratio, they both can be used and an estimation of the precision of the measurement can be carried out. However there are cases, depending on the relative orientation of the crystal with respect to the electric field, where either S_1 or S_2 vanishes. In those cases, only one signal is used.

D. Front-end electronics

To perform accurate polarimetry measurements, it is necessary to detect very small variations of light intensity over an intense, continuous signal. To do this effectively, avalanche photodiode (APD) transducers have been employed, and a specific front-end electronics has been developed (see Ref. 42 for another comparable solution). Since APDs are more affected by noise than standard photodiodes and their response is dependent upon the temperature, a proper voltage feeder has been developed as depicted in Fig. 6. On the other hand, APDs are much more sensitive than the standard photodiodes.

The DC feeder compensates the effects of variations of temperature so that the gain of the APD remains constant. A closed-loop control guarantees the accuracy of the feeding system.

To expand the small variations of the current flowing through the APD, a proper feedback loop has been developed for subtracting the continuous, or slowly varying, component of the current. The result is then converted into a voltage signal through an I/V converter and filtered using an analogic filter with a bandwidth of 75 MHz. The control loop also makes the slowly varying reference available. This measure is very important since, due to small misalignments, the continuous light intensity through the four channels may be different, giving artifacts in the results. The measurement of the continuous intensity makes it possible to effectively and in real-time compensate these issues.

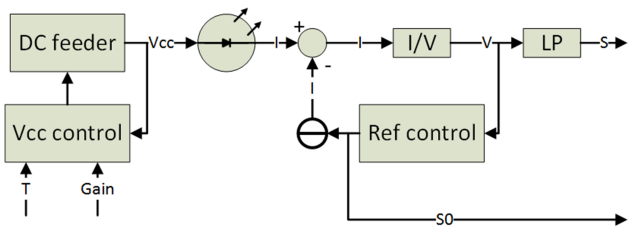

FIG. 6. Conceptual scheme of the measurement electronics described in the text.

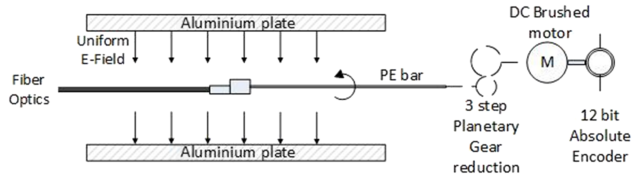

FIG. 7. The experimental setup.

E. Laboratory tests

The sensor assembly, depicted in Fig. 2, has been placed between two metallic plates as detailed in Fig. 7. One has been grounded and the other connected to a power supply, either an impulse generator or an AC source at 50 Hz. In the first case, a Haefely P35 impulse generator has been used, while in the second one a PIVI TMO/128 transformer has been coupled to a low voltage A.M.E. CCU-1-50/75/100 power supply.

The metallic plates have been placed 10 cm from the sensor, and their dimensions (50 cm × 50 cm) have been chosen in such a way that the electric field is uniform in the central part, i.e., in the region where the sensor is placed. The sensor head has been suspended to a 50 cm long polyethylene bar, which can be rotated with a relatively high precision. The bar itself is attached to an electric motor through a three-step gear reduction. The angle has been measured with a 12-bit encoder. The error of this positioning system is about ±2° due to the mechanical backslashes in the planetary gear. The five optic fibers have been connected to the electronic unit that holds the laser beam source and all the analogic readout electronics. This unit produces eight signals (four variable signals and four continuous reference signals) as depicted schematically in Fig. 6, and they are digitalized using a PXI-NI5124 unit (for the variable signals) and a PXI-6025E unit (for the continuous signals).

In the first test, the sensor has been fixed with the x axis of the crystal aligned with the direction of the electric field (see Fig. 4). We have first considered a lightning waveform described in the IEC 60060-1 standard which has a large bandwidth in the range 10 kHz-1 MHz. The aim of this test is to verify that the sensor is capable of reproducing all the spectral components in this range. The results are shown in Fig. 8 and prove that our system correctly reproduces the rising and falling fronts of the impulse, i.e., both the higher and lower frequencies.

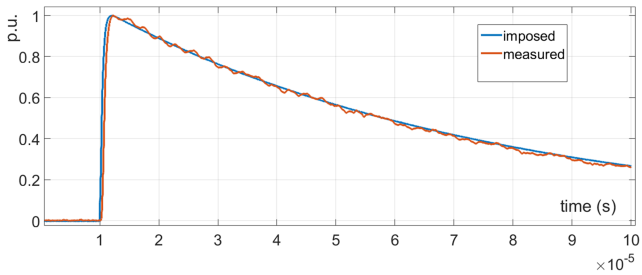

FIG. 8. Comparison between the imposed electric field and the measured electric field using an impulse waveform.

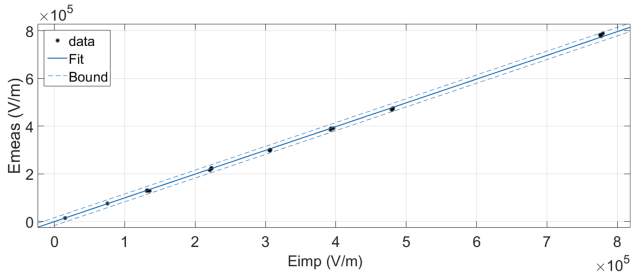

FIG. 9. Linearity of the response of the signal versus the applied electric field. Eimp is the imposed electric field and Emeas is the measured electric field.

The same configuration has been used to test the linearity response of the sensor by imposing electric fields in the range from 20 kV/m to 800 kV/m. Eight voltage levels have been chosen and four acquisitions have been performed for each value. Then a regression curve has been computed as depicted in Fig. 9. All the measurements lay within the 99% confidence level.

It is also interesting to check the dependence of the modulus of the measured electric field upon the angle and the ability of the sensor to correctly recover the direction of the electric field. The sensor has been rotated as displayed in Fig. 7 from zero to 2π radiants with an increment of 0.0873 radiant (5°). For each angle, three measurements have been acquired. Results are shown in Fig. 10. As stated in Sec. II C, when the signal to noise ratio is high enough, two samplings of the electric field magnitude are performed for each measurement. Sometimes, due to the relative orientation of the sensor

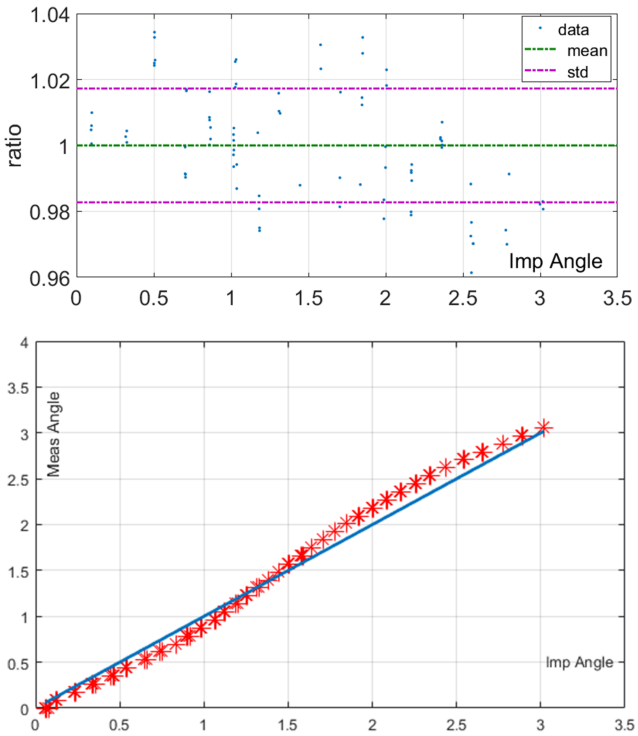

FIG. 10. Ratio between the measured electric field and the imposed electric field considering different angles (upper figure) and the imposed (Imp) angle against the measured angle (Meas).

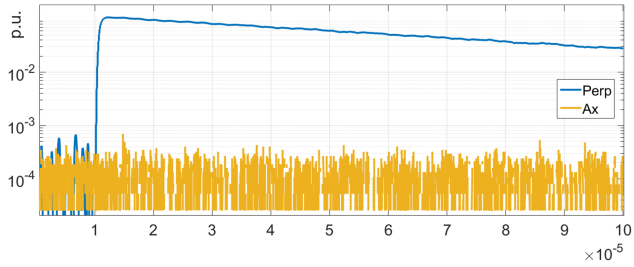

FIG. 11. Intensity of the electric signal produced by one of the APDs when the electric field is perpendicular to the laser beam (Perp) and when the electric field is aligned with the laser beam (Ax).

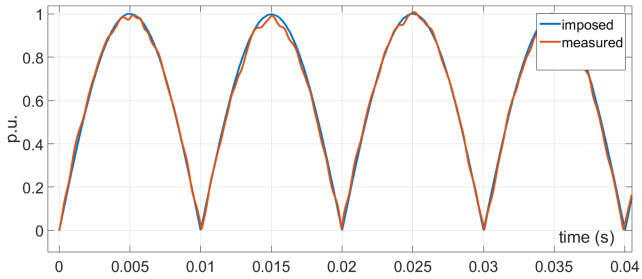

FIG. 12. Comparison between the imposed electric field and the measured electric field using a 50 Hz signal.

with respect to the electric field, one acquisition may show a small signal to noise ratio and it is discarded. Therefore each angle might have a different number of data acquisitions in the range (6-3).

The error with respect to the electric field direction is below 3%, and the electric field modulus is almost independent of the angle: the standard deviation is smaller than 2%.

We have also tested the ability of the sensor to reject the component of the electric field aligned with the *z*-axis of the crystal. The electric motor, the gear, and the polyethylene bar have been removed, and the sensor has been placed and fixed on the ground plate with either the z-axis or the x-axis of the crystal aligned with the electric field. The signals acquired by one of the APDs, using either the x or z orientation, have been compared and are shown in Fig. 11. The ratio between the results obtained in the two configurations spans more than three decades, and this result represents a significant improvement over the results reported in Ref. 30.

Finally, we have connected the plates of the capacitor to an AC power supply and compared the measured electric field with the imposed one. The results shown in Fig. 12 prove that the field is correctly recovered in terms of phase and amplitude.

III. CONCLUSIONS

In this work, we have described a novel technique for the measurement of two components of the vector electric field. The main difference with respect to other polarimetry methods presented in the literature is the direction of the laser beam in the crystal which is aligned with the extraordinary axis. Moreover, dedicated electronics appreciably increment the sensitivity of the system.

The sensor constitutes a prototype built without using any high precision alignment device, and therefore, the sensing unit is relatively large to facilitate its construction. Big improvements are possible for increasing the signal to noise ratio. In spite of this, the performances are remarkable, providing a very high linearity and an error on angle determination below 3%. The spectral bandwidth is also very good since the system is capable of representing both very fast and slow waveforms and reproducing signals with both fast and relatively slow components. Finally, the rejection of the electric field component along the *z* axis is very performant and matches or exceeds the performances of the devices already presented in the literature.[25,30]

Finally, the technology described in this work allows us to use a larger class of optical crystals preserving good, and still improvable, performances.

ACKNOWLEDGMENTS

This work has been financed by the Research Fund for the Italian Electrical System under the Contract Agreement between RSE and the Ministry of Economic Development. The authors wish to thank L. Barbareschi for her valuable contribution and suggestions.

[1] A. Cavallini, R. Ciani, M. Conti, P. F. H. Morshuis, and G. C. Montanari, "Modeling memory phenomena for partial discharge processes in insulation cavities," in *Annual Report of Conference on Electrical Insulation and Dielectric Phenomena* (IEEE, 2003), pp. 723–727.

[2] A. Cavallini, G. C. Montanari, M. Tozzi, and X. Chen, "Diagnostic of HVDC systems using partial discharges," IEEE Trans. Dielectr. Electr. Insul. **18**(1), 275–284 (2011).

[3] L. Barbieri, A. Villa, and R. Malgesini, "A step forward in the characterization of the partial discharge phenomenon and the degradation of insulating materials through nonlinear analysis of time series," IEEE Electr. Insul. Mag. **28**(4), 14–21 (2012).

[4] C. Volat, L. Duvillaret, and G. Gaborit, "Detection of AC corona discharges using an electro-optic E-field sensor," in *Electrical Insulation (ISEI), Conference Record of the 2012 IEEE International Symposium* (IEEE, 2012), pp. 95–98.

[5] S. Abdel-Sattar and H. Singer, "Saturated corona profiles at ground surfaces and underneath HVDC lines," IEEE Trans. Electr. Insul. **25**(6), 1138–1144 (1990).

[6] A. Villa, L. Barbieri, M. Gondola, A. R. Leon-Garzon, and M. Malgesini, "An efficient algorithm for corona simulation with complex chemical models," J. Comput. Phys. **337**, 233 (2017).

[7] F. Lecoche, G. Gaborit, L. Gillette, G. Schmitt, A. Grau, and L. Duvillaret, "Contactless, real time, and vectorial inspection of a multiwire power cable voltage using an electro-optic technique," IEEE Sens. J. **14**(8), 2881–2888 (2014).

[8] Y. Murooka and T. Nakano, "Optical high-sensitive field sensor using a Pockels crystal," Rev. Sci. Instrum. **63**(12), 5582 (1992).

[9] L. Gillette *et al.*, "Optical sensor for the diagnostic of high voltage equipment," in *Electrical Insulation Conference (EIC)* (IEEE, 2014), pp. 142–146.

[10] G. Gaborit, P. Jarrige, F. Lecoche, J. Dahdah, and L. Duvillaret, "Spatiotemporal and vectorial analysis of the electric field vector with an optical sensor," in *2014 IEEE Conference on Antenna Measurements & Applications (CAMA), Antibes Juan-les-Pins, France, 16–19 November 2014* (IEEE, 2014), pp. 1–3.

[11] R. Zeng, C. Zhuang, Z. Yu, Z. Li, and Y. Geng, "Electric field step in air gap streamer discharges," Appl. Phys. Lett. **99**(22), 221503 (2011).

[12] K. Yang, G. David, J.-G. Yook, I. Papapolymerou, L. P. B. Katehi, and J. F. Whitaker, "Electrooptic mapping and finite-element modeling of the near-field pattern of a microstrip patch antenna," IEEE Trans. Microwave Theory Tech. **48**(2), 288–294 (2000).

[13]J. E. Toney, V. E. Stenger, S. A. Kingsley, A. Pollick, S. Sriram, and E. Taylor, "Advanced materials and device technology for photonic electric field sensors," Proc. SPIE **8519**, 851904 (2012).
[14]R. Zeng, B. Wang, B. Niu, and Z. Yu, "Development and application of integrated optical sensors for intense e-field measurement," Sensors **12**(8), 11406–11434 (2012).
[15]L. Duvillaret, S. Rialland, and J.-L. Coutaz, "Electro-optic sensors for electric field measurements. I. Theoretical comparison among different modulation techniques," J. Opt. Soc. Am. B **19**(11), 2692 (2002).
[16]L. Duvillaret, S. Rialland, and J.-L. Coutaz, "Electro-optic sensors for electric field measurements. II. Choice of the crystals and complete optimization of their orientation," J. Opt. Soc. Am. B **19**(11), 2704 (2002).
[17]S. Mathews, G. Farrell, and Y. Semenova, "All-fiber polarimetric electric field sensing using liquid crystal infiltrated photonic crystal fibers," Sens. Actuators, A **167**(1), 54–59 (2011).
[18]S. Mathews, G. Farrell, and Y. Semenova, "Liquid crystal infiltrated photonic crystal fibers for electric field intensity measurements," Appl. Opt. **50**(17), 2628 (2011).
[19]Z. Fuwen, C. Fushen, and F. Lei, "The research on the electric field sensor with no electrode in x-cut LiNbO/sub 3/," in *IEEE 2002 International Conference on Communications, Circuits and Systems and West Sino Expositions, 19 February 2003* (IEEE, 2003).
[20]S. Chadderdon *et al.*, "Electric-field sensors utilizing coupling between a D-fiber and an electro-optic polymer slab," Appl. Opt. **50**(20), 3505–3512 (2011).
[21]R. S. Gibson, "Slab coupled optical fiber sensors for electric field sensing applications" (Department of Electrical and Computer Engineering, Brigham Young University, 2009).
[22]S. Chadderdon, D. Perry, J. Van Wagoner, R. Selfridge, and S. Schultz, "Multi-axis all dielectric electric field sensors," Proc. SPIE **8376**, 837608 (2012).
[23]M. Bernier, A. Warzecha, L. Duvillaret, J. L. Lasserre, and A. Paupert, "Fully automated E-field measurement setup using pigtailed electro-optic sensors for accurate, vectorial, and reliable remote measurement of high-power microwave signals," Proc. SPIE **7114**, 71140L–1 (2008).
[24]M. Bernier, G. Gaborit, L. Duvillaret, A. Paupert, and J. L. Lasserre, "Electric field and temperature measurement using ultra wide bandwidth pigtailed electro-optic probes," Appl. Opt. **47**(13), 2470–2476 (2008).
[25]G. Gaborit *et al.*, "A nonperturbative electrooptic sensor for *in situ* electric discharge characterization," IEEE Trans. Plasma Sci. **41**(10), 2851–2857 (2013).
[26]Y. Gaeremynck, P. Jarrige, L. Duvillaret, G. Gaborit, and F. Lecoche, "Two-components electric-field sensor for ultra wide band polarimetric measurements," in *Progress in Electromagnetics Research Symposium Proceedings, Marrakesh, Morocco, 20–23 March 2011*, p. 1749.
[27]G. Gaborit, G. Martin, L. Duvillaret, B. Crabos, and J. L. Lasserre, "Advantages and potentialities of electro-optic sensors for an ultra wide bandwidth characterization of radiated or guided electric fields," in European Test & Telemetry Conference, Toulouse, France.
[28]G. Gaborit *et al.*, "Single shot and vectorial characterization of intense electric field in various environments with pigtailed electrooptic probe," IEEE Trans. Plasma Sci. **42**(5), 1265–1273 (2014).
[29]G. Gaborit, J. L. Coutaz, and L. Duvillaret, "Vectorial electric field measurement using isotropic electro-optic crystals," Appl. Phys. Lett. **90**(24), 241118 (2007).
[30]Y. Gaeremynck, G. Gaborit, L. Duvillaret, M. Ruaro, and F. Lecoche, "Two electric-field components measurement using a 2-port pigtailed electro-optic sensor," Appl. Phys. Lett. **99**(14), 141102 (2011).
[31]P. Jarrige, J. Dahdah, F. Lecoche, L. Duvillaret, G. Gaborit, and L. Gillette, "Optical antennas for a complete electric field characterization," in *2015 IEEE Electrical Insulation Conference (EIC), Seattle, WA, 7–10 June 2015* (IEEE, 2015), pp. 471–474.
[32]W. K. Kuo, Y. T. Huang, and S. L. Huang, "Three-dimensional electric-field vector measurement with an electro-optic sensing technique," Opt. Lett. **24**(22), 1546–1548 (1999).
[33]G. Gaborit *et al.*, "Electrooptic probe based on an organic microcavity," IEEE Photonics Technol. Lett. **17**(10), 2140–2142 (2005).
[34]X. Zheng *et al.*, "Electro-optic sampling system with a single-crystal 4-N, N-dimethylamino-4′-N′-methyl-4-stilbazolium tosylate sensor," Appl. Phys. Lett. **82**(15), 2383–2385 (2003).
[35]M. Jazbinsek, L. Mutter, and P. Gunter, "Photonic applications with the organic nonlinear optical crystal DAST," IEEE J. Sel. Top. Quantum Electron. **14**(5), 1298–1311 (2008).
[36]T. R. Sliker and J. M. Jost, "Linear electro-optic effect and refractive indices of cubic ZnTe*," J. Opt. Soc. Am. **56**(1), 130–131 (1966).
[37]F. Pan, X. Xiao, Y. Xu, and S. Ren, "Optical AC voltage sensor based on two< formula formulatype=," IEEE Trans. Instrum. Meas. **61**(4), 1125–1129, (2012).
[38]H. Matsumoto, S. Matsuoka, A. Kumada, and K. Hidaka, "Suppression of piezoelectric vibration on Pockels crystal," in *Transmission and Distribution Conference and Exposition: Asia and Pacific* (IEEE, 2009), pp. 1–4.
[39]D. N. Nikogosyan, "Beta barium borate (BBO)," Appl. Phys. A: Solids Surf. **52**(6), 359–368 (1991).
[40]A. Yariv and P. Yeh, *Optical Waves in Crystals: Propagation and Control of Laser Radiation* (Wiley, New York, 1984).
[41]T.-C. Poon and T. Kim, *Engineering Optics with Matlab* (World Scientific, Hackensack, N.J., 2006).
[42]A. Pullia, T. Sanvito, M. A. Potenza, and F. Zocca, "A low-noise large dynamic-range readout suitable for laser spectroscopy with photodiodes," Rev. Sci. Instrum. **83**(10), 104704 (2012).